Journal of Alloys and Compounds 480 (2009) 171–183

Contents lists available at ScienceDirect

Journal of Alloys and Compounds

journal homepage: www.elsevier.com/locate/jallcom

A neutron diffraction study of the hexagonal pseudo-ternary compounds $ErMn_{6-x}Fe_xSn_6$ ($x = 0.2, 0.4, 0.6, 0.8, 1.0, 2.0, 3.0, 4.0$)

J. Bourgeois, G. Venturini*, B. Malaman

Laboratoire de Chimie du Solide Minéral, Université Henri Poincaré-Nancy I, associé au CNRS (UMR 7555), B.P. 239, 54506 Vandoeuvre les Nancy Cedex, France

ARTICLE INFO

Article history:
Received 19 January 2009
Received in revised form 28 January 2009
Accepted 29 January 2009
Available online 7 February 2009

Keywords:
Rare earth alloys and compounds
Transition metal alloys and compounds
Magnetically ordered materials
Magnetisation
Neutron diffraction

ABSTRACT

The hexagonal $ErMn_{6-x}Fe_xSn_6$ solid solution ($0.2 < x < 4$) has been studied by magnetisation measurements and neutron diffraction. The ordering temperature of the T = (Mn,Fe) sublattice almost continuously increases from $T = 386$ K for $x = 0.2$ to $T = 498$ K for $x = 4$. The T sublattice orders in the successive magnetic structures helimagnetic H1, antiferromagnetic AF2, helimagnetic H2 and antiferromagnetic AF1 with increasing iron content. While structures AF2 and H1 were already observed in ternary Mn compounds and AF1 in ternary iron compounds, the structure H2 is of a new kind characterized by an AF slab around the Er(1a) site. At low temperature, a change of the easy direction of the Er moment from easy plane to easy axis is observed. The iron-rich compounds display a ferromagnetic order of the Er sublattice. A new kind of magnetic structure characterized by a sine-wave modulated arrangement with a propagating vector $Q = (0, 0, q_z)$ is also observed. The evolution of the magnetic properties (enhancement of the AF character of the (Mn,Fe) sublattice and magnetocrystalline anisotropy of erbium) is discussed.

1. Introduction

The RT_6Sn_6 compounds (R = heavy rare earth element, T = Fe,Mn) have been extensively studied in relation with the complicated interplay between the magnetic properties of the R and T sublattices [1–11]. The manganese compounds crystallize in the simple hexagonal structure $HfFe_6Ge_6$ which can be viewed as a stacking of two different slabs: the Mn–Sn–Sn–Sn–Mn slab and the Mn–(Sn,R)–Mn slab. On another hand the iron compounds crystallize either in the hexagonal structure or in various more or less complicated orthorhombic structures [12]. The structural evolution in the iron compounds seems to be related to a geometrical effect since the smallest R elements (Tm–Lu) give rise to the stabilisation of the hexagonal structure whereas the orthorhombic structures are stable in systems containing the largest R elements (Gd–Er). From this analysis, it was expected that the relatively small erbium atom would lead to a hexagonal $ErMn_{6-x}Fe_xSn_6$ solid solution with a rather large homogeneity range.

These compounds order magnetically into ferromagnetic Mn or Fe Kagomé planes but the interplane couplings in the manganese and iron compounds are quite different. The three-dimensional order in the manganese stannides is either ferrimagnetic (Gd–Ho, Er below 62 K), helimagnetic H1 (Er above 62 K, Tm below 324 K) or antiferromagnetic AF2 (Tm above 324 K) [1–6]. In the three kinds of magnetic structure, it is observed that the arrangement of the Mn moments in the Mn–Sn–Sn–Sn–Mn slab is parallel or almost parallel while a more or less large angle between the Mn moments prevails in the Mn–(Sn,R)–Mn slab. In the contrary, the hexagonal iron compounds are characterized by antiferromagnetic Fe–Sn–Sn–Sn–Fe and Fe–(R,Sn)–Fe slabs (AF1) and the orthorhombic iron compounds also display an antiparallel arrangement between the pseudo-hexagonal Fe planes [7–11].

For this reason it was interesting to undertake a neutron diffraction study on a manganese iron solid solution in order to check the evolution of the magnetic arrangements. Moreover, a recent magnetic study on the $HoMn_{6-x}Fe_xSn_6$ solid solution ($0 \leq x \leq 1.2$) has shown, in spite of the limited studied range, consequent changes of the magnetic behaviour [13].

2. Experimental procedures

The samples have been prepared in an induction furnace starting from stoichiometric amounts of the elements. The resulting ingot is annealed at 1123 K during one week and checked by X-ray powder analysis (Xpert Pro diffractometer Cu Kα). The weak impurity lines detected are those of elemental tin, $(Mn,Fe)Sn_2$ ($CuAl_2$-type) and $(Mn,Fe)_{2-x}Sn$ (Ni_2In-type).

The magnetisation measurements have been performed on a MANICS magnetosusceptometer in the temperature range 4.2–600 K and in fields up to 1.5 T.

The neutron diffraction patterns have been recorded on the D1B diffractometer at the Institut Laue Langevin (Grenoble) using the wavelength ($\lambda = 2.520$ Å). Long duration patterns have been recorded at 300 and 2 K and short duration patterns in the 2–300 K temperature range. The structures have been refined using the Fullprof software [14].

* Corresponding author. Tel.: +33 3 83 68 46 73; fax: +33 3 83 68 46 11.
E-mail address: Gerard.Venturini@lcsm.uhp-nancy.fr (G. Venturini).

0925-8388/$ – see front matter © 2009 Elsevier B.V. All rights reserved.
doi:10.1016/j.jallcom.2009.01.120

Table 1
Cell parameters measured at room temperature and main magnetic data of the compounds $ErMn_{6-x}Fe_xSn_6$.

	a (Å)	c (Å)	c/a	V (Å^3)	T_N (K)	T_c (K)	T_{AF-H1} (K)
$ErMn_{5.8}Fe_{0.2}Sn_6$	5.510(1)	8.996(2)	1.6327	236.5	386	–	341
$ErMn_{5.6}Fe_{0.4}Sn_6$	5.505(1)	8.993(2)	1.6336	236.0	421	–	
$ErMn_{5.4}Fe_{0.6}Sn_6$	5.498(1)	8.990(2)	1.6351	235.3	445	–	
$ErMn_{5.2}Fe_{0.8}Sn_6$	5.493(1)	8.987(2)	1.6381	234.8	458	–	
$ErMn_5FeSn_6$	5.488(1)	8.983(2)	1.6370	234.3	470	–	
$ErMn_4Fe_2Sn_6$	5.464(1)	8.971(2)	1.6417	231.9	501	37	
$ErMn_3Fe_3Sn_6$	5.442(1)	8.955(2)	1.6455	229.7	490	26	
$ErMn_2Fe_4Sn_6$	5.425(1)	8.941(2)	1.6479	227.9	498	20	

3. Structural data

The analysis of the X-rays powder diffraction data shows that the compounds $ErMn_{6-x}Fe_xSn_6$ crystallize in the hexagonal $HfFe_6Ge_6$-type structure up to $x=4$ while the compound $ErMnFe_5Sn_6$ is isotypic of the orthorhombic $ErFe_6Sn_6$ structure. Therefore, the replacement of manganese by iron leads to $HfFe_6Ge_6$-type solid solution with a rather large extent, a feature which should fairly enable a study of the magnetic properties as a function of the iron substitution. The cell parameters are gathered in Table 1 and a representation of the crystal structure is given in Fig. 1.

4. Magnetic measurements

Fig. 2 displays the thermal variation of the magnetisation of the compounds $ErMn_{6-x}Fe_xSn_6$ and the transition temperatures are summarized in Table 1. The compounds of the whole series order antiferromagnetically and their Néel temperatures globally increase with the iron concentration from 386 K for $x=0.2$ to 498 K for $x=4$. The thermomagnetic curves clearly display a peak at the ordering point except for $ErMn_{5.8}Fe_{0.2}Sn_6$ for which a plateau region is observed. According to the magnetic behaviour of $TmMn_6Sn_6$ [6], it is strongly suggested that the right part of the plateau is related to the transition from the paramagnetic state to the AF state and the left part to the transition from AF to helimagnetic state. Other magnetic transitions are mainly observed for the compounds $ErMn_4Fe_2Sn_6$, $ErMn_3Fe_3Sn_6$ and $ErMn_2Fe_4Sn_6$ whose magnetisation curves display a strong increase upon cooling at low temperature. The transitions observed around $T\approx250$ K for the compounds $ErMn_{5.8}Fe_{0.2}Sn_6$, $ErMn_{5.6}Fe_{0.4}Sn_6$, $ErMn_{5.4}Fe_{0.6}Sn_6$ and $ErMn_{5.2}Fe_{0.8}Sn_6$ should be related to the ferromagnetic Ni_2In-type impurities [15].

The isotherm curves recorded at 4.2 K show that the magnetisation of the compounds $ErMn_4Fe_2Sn_6$, $ErMn_3Fe_3Sn_6$ and $ErMn_2Fe_4Sn_6$ displays a ferro(ferri)magnetic-like behaviour with more or less large remanent magnetisation (Fig. 3). For these compounds, the saturation value increases with the iron content from 2.5 to 4.5μ_B/f.u. The magnetisation value of the compound $ErMn_5FeSn_6$ also reaches a relatively large value (2.5μ_B/f.u.) but without saturation. The compound $ErMn_{5.8}Fe_{0.2}Sn_6$ displays a metamagnetic-like behaviour and hysteresis effect. The critical field is close to 1.2 T and the magnetisation reaches a maximum value of 2.5μ_B/f.u., close to the magnetisation of the ferrimagnetic compound $ErMn_6Sn_6$ [5]. Therefore, it may be inferred that the applied field induces a transition to the ferrimagnetic state. The curves of the other compounds $ErMn_{5.6}Fe_{0.4}Sn_6$, $ErMn_{5.4}Fe_{0.6}Sn_6$

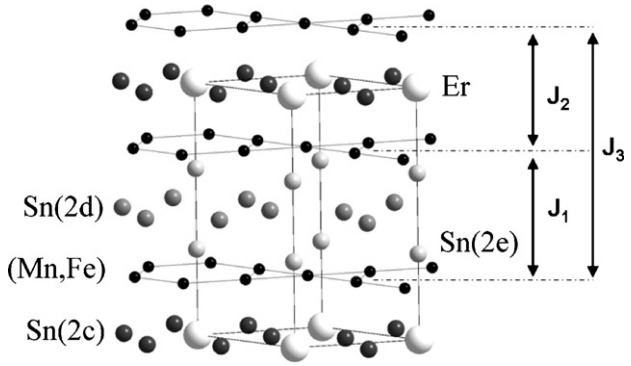

Fig. 1. A view of the $HfFe_6Ge_6$-type structure.

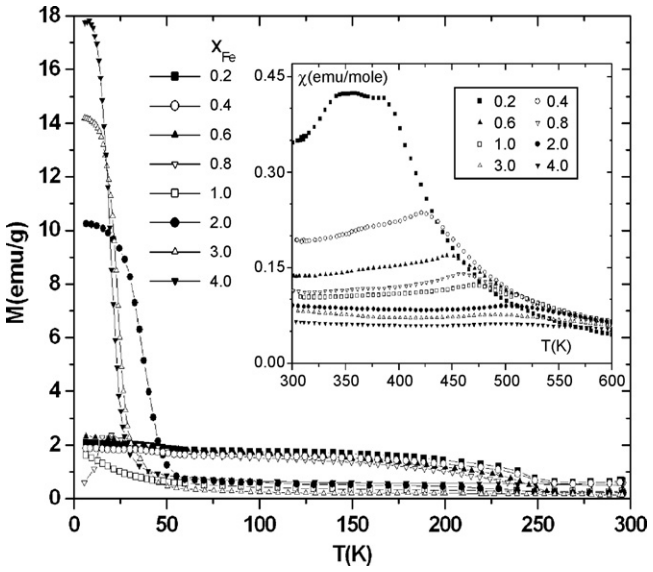

Fig. 2. Thermomagnetic curves of the $ErMn_{6-x}Fe_xSn_6$ compounds (inset shows the high temperature behaviour).

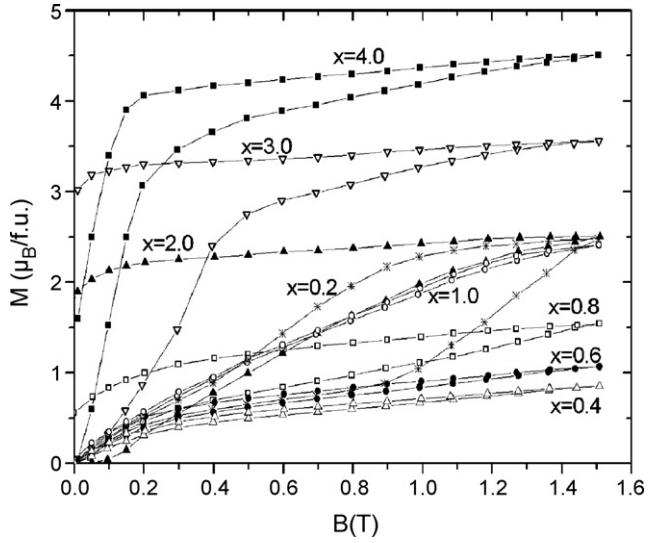

Fig. 3. Magnetisation curves of the $ErMn_{6-x}Fe_xSn_6$ compounds recorded at 4.2 K.

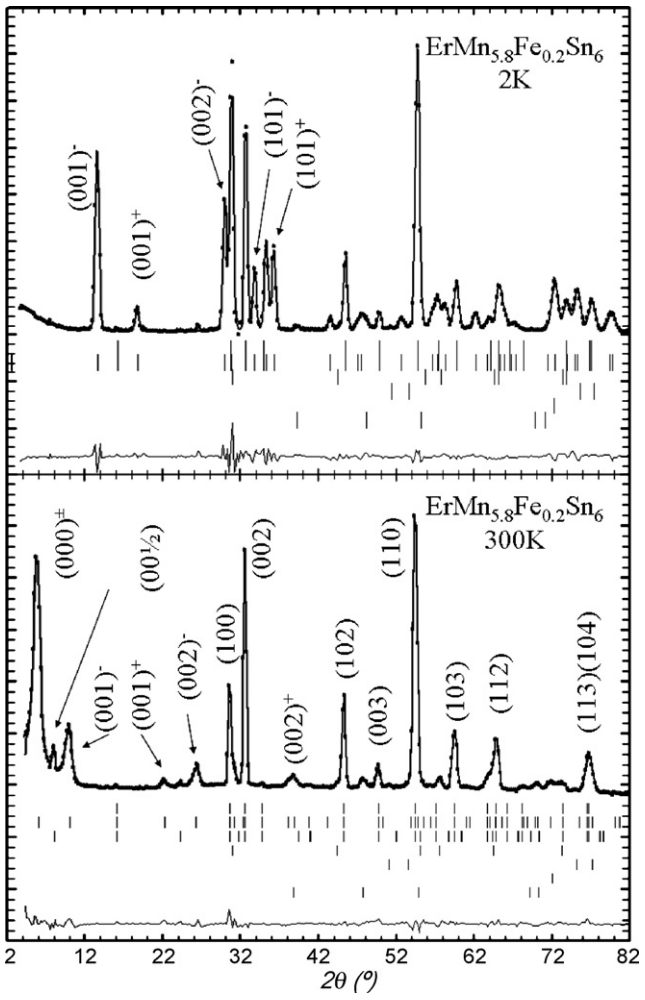

Fig. 4. Observed and calculated neutron diffraction patterns of $ErMn_{5.8}Fe_{0.2}Sn_6$ at 300 and 2 K (extra lines; from bottom to top: Ni_2In-type $T_{2-x}Sn$; sample holder; elemental tin; $CuAl_2$-type TSn_2).

and $ErMn_{5.2}Fe_{0.8}Sn_6$ display a small spontaneous magnetisation which accounts for the presence of the Ni_2In-type impurities.

5. Neutron diffraction study of $ErMn_{5.8}Fe_{0.2}Sn_6$

The neutron diffraction patterns of this compound (Fig. 4) are mainly characterized by additional magnetic peaks which can be indexed as satellites of the nuclear ones with a propagating vector $Q=(0, 0, q_z)$ as already observed in $ErMn_6Sn_6$ [2]. However, these lines remain down to 2 K while $ErMn_6Sn_6$ was characterized by a transition from the helimagnetic state to a ferrimagnetic state at 62 K. The pattern recorded at 300 K shows an additional weak line around $2\theta = 8^\circ$ which may be indexed as (0, 0, 1/2). This line should be a reminiscence of a high temperature antiferromagnetic structure AF2 not observed in $ErMn_6Sn_6$, but already observed in $TmMn_6Sn_6$ above 324 K [16]. According to the short duration patterns recorded in the intermediate temperature range, this line decreases upon cooling and becomes negligible below 275 K.

The refinements of the magnetic structures from the patterns recorded at 300 and 2 K have been done considering the classical helimagnetic structure (H1) of the RMn_6Sn_6 compounds [2]. The refined magnetic parameters are the magnitude of the moment on the (Mn,Fe) site, the magnitude of the erbium moment, the angle θ between the normal to the helical plane and the c-axis and the phase angle of the (Mn,Fe) moments defined as ϕ_T for (Mn,Fe) atoms lying at $z \approx 1/4$ and $-\phi_T$ for (Mn,Fe) atoms lying at $z \approx 3/4$. The results of the refinement are given in Table 2 and the observed and calculated patterns are displayed in Fig. 4. A representation of the magnetic structure is given in Fig. 5a. The projection of the structure along the [0 0 1] direction, given in Fig. 6a, allows a better view of the relative orientation of the moments in the successive (0 0 1) planes.

Table 2
Refined parameters of $ErMn_{5.8}Fe_{0.2}Sn_6$ at 300 and 2 K.

	300 K	2 K
a (Å)	5.410(1)	5.481(1)
c (Å)	8.994(2)	8.964(2)
z_{Fe}	0.245(1)	0.246(1)
z_{Sn}	0.333(1)	0.338(1)
$m_{Fe}[m_{Mn}]$	0.028[0.972](4)	0.028[0.972]
Helimagnetic 1		
μ_{T1} (μ_B)	1.99(4)	2.32(3)
μ_{Er1} (μ_B)	1.36(8)	8.92(8)
θ_{T1} (°)	38(1)	16(2)
ϕ_{T1} (°)	213.2(6)	192.6(4)
q_{z1} (r.l.u.)	0.3752(5)	0.1580(2)
Commensurate		
μ_T (μ_B)	0.27(1)	–
θ_T (°)	90	–
$\mu_{T\,total}$ (μ_B)	2.01	2.32
$\mu_{Er\,total}$ (μ_B)	1.36	8.92
R_{Bragg}, R_F	3.58; 3.68	3.08; 3.46
R_{magn}	4.18;10.9	4.96; –
R_{wp}, R_{exp}, χ^2	7.0; 1.2; 33	9.5; 0.9; 115

These relative orientations of the moments in the successive planes along [0 0 1] are given by the following expressions:

$$\alpha_{Er}(\text{at } z_{Er} = n) = 2\pi q_z z_{Er}$$
$$\alpha_{T1}(\text{at } z_T \approx n + 1/4) = 2\pi q_z z_T + \phi_T$$
$$\alpha_{T2}(\text{at } z_T \approx n + 3/4) = 2\pi q_z z_T - \phi_T$$

These expressions enable the calculation of the angle between the moments T = (Mn,Fe) belonging to the T–Sn–Sn–Sn–T and T–(Sn,Er)–T slabs. The thermal variation of these angles is displayed in Fig. 7. The angle between the T moments belonging to the T–Sn–Sn–Sn–T slab is small and does not greatly vary in the whole studied temperature range thus indicating that this slab is almost ferromagnetic. The angle between the T moments belonging to the T–(Sn,Er)–T slab decreases upon cooling following the q_z variation. In the whole temperature range, this angle is smaller than 180° so that the erbium site experiences a molecular field coming from the T sublattice. In counterpart, the Er moment displays a non-zero value in the whole 2–300 K although a value close to the theoretical free ion value is only observed at low temperature (Fig. 8).

5.1. Neutron diffraction study of $ErMn_{5.6}Fe_{0.4}Sn_6$

The pattern recorded at 300 K (Fig. 9) displays the characteristic lines of the antiferromagnetic structure AF2 (Fig. 5b) stable at high temperature for $TmMn_6Sn_6$ and for most of the germanides RMn_6Ge_6 [16,17]. This magnetic structure is characterized by a doubling of the c-axis and by the magnetic peaks ($h\,k\,l$) where l is half-integer. The moment arrangement observed in the other known representatives is characterized by a ferromagnetic chemical cell, the moments changing their sign in the adjacent chemical cells along [0 0 1]. The refinement has been undertaken on the basis of this kind of arrangement. The refined parameters are the magnitude of the (Mn,Fe) moment and its orientation with respect to the [0 0 1] direction. It leads to a residual factor $R = 7.6\%$ with the moment lying in the (0 0 1) plane. An attempt with the second possible model based on an antiferromagnetic chemical cell leads to

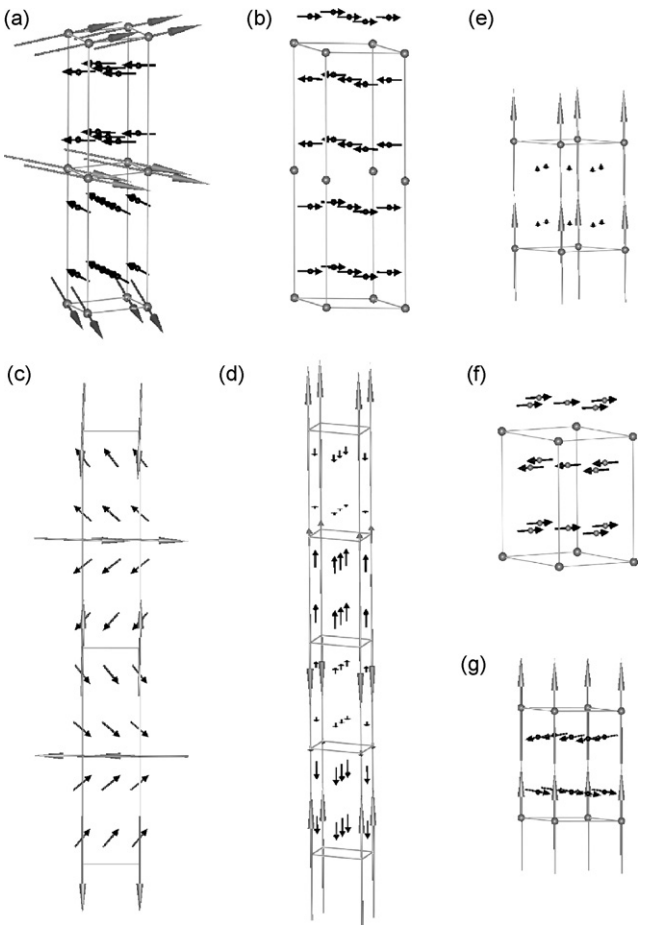

Fig. 5. View of the magnetic arrangements observed for the $ErMn_{6-x}Fe_xSn_6$ compounds (a) H1 structure with moments in the (0 0 1) plane, (b) AF2 structure with moments in the (0 0 1) plane, (c) $H1_2$ structure with the normal to the helical plane perpendicular to the [0 0 1] direction, (d) sine-modulated structure with moments along [0 0 1], (e) ferromagnetic arrangement of erbium moments with a small opposite component on the T sublattice, (f) AF1 structure with moments in the (0 0 1) plane and (g) ferromagnetic structure of erbium moment and canted AF1 structure for T moment.

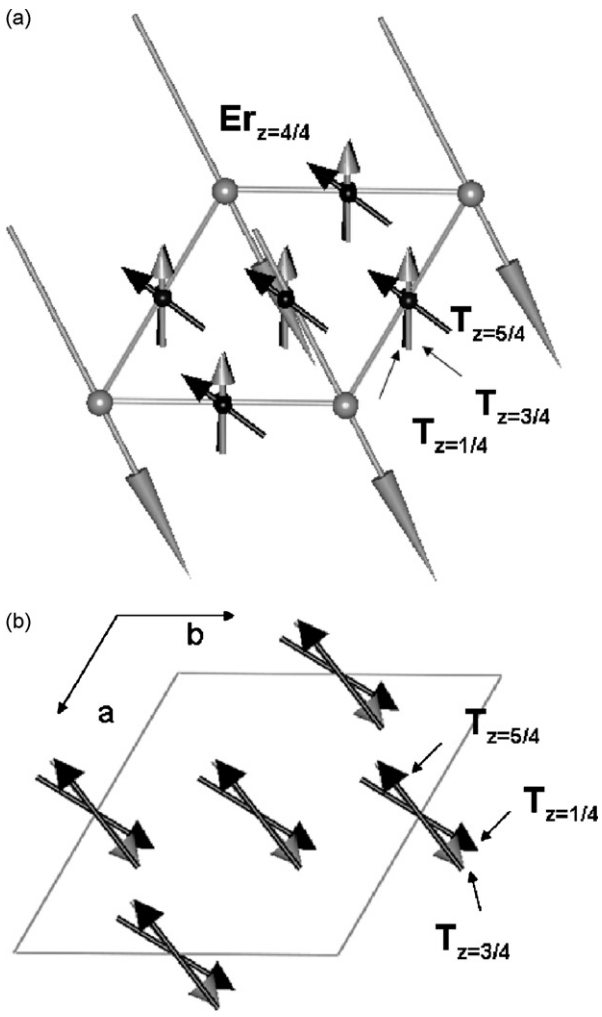

Fig. 6. Projection of the helimagnetic structures H1 (a) and H2 (b).

the slightly higher residual factor $R = 9.3\%$. The final parameters, refined with the first model, are gathered in Table 3 and the magnetic structure is drawn in Fig. 5b.

A complicated evolution takes place upon cooling (Fig. 10). Below $T \approx 175$ K, shoulders appear at the feet of the (0 0 1/2) line. These shoulders develop into a couple of satellites around $T \approx 150$ K and down to $T \approx 70$ K. In this temperature range, the shape of the satellites is strongly asymmetric. Below $T \approx 50$ K, a second set of satellites takes place besides the previous set. Simultaneously, the (0 0 1/2) line intensity decreases from $T \approx 175$ K to $T \approx 70$ K and vanishes below $T \approx 50$ K.

The magnetic structures have been refined at 2 K considering a mixture of two helimagnetic arrangements $H1_1$ and $H1_2$ with different propagating vectors. For each structure, the q_z component, the magnitude of the Er and (Mn,Fe) moments, the phase angle ϕ_T and the orientation of the helical plane θ have been refined. The results are given in Table 3 and the observed and calculated patterns are displayed in Fig. 9. The magnetic structures $H1_1$ and $H1_2$ are characterized by propagating vectors whom q_z component is close to 1/6 and 1/4. The value of the angle θ are refined close to 0° and 90° for $H1_1$ and $H1_2$ respectively and have been fixed to these values in the final refinements. The values of the propagating vector and phase angle enable the calculation of the angle between the moments of (Mn,Fe) in the T–Sn–Sn–Sn–T and T–(Er,Sn)–T slabs. For the structure $H1_1$, these angles are 7° and 54° respectively, and for the structure $H1_2$ 9° and 81°. Therefore, the moments are still almost parallel in the T–Sn–Sn–Sn–T slab. A representation of the magnetic structure $H1_2$ is given in Fig. 5c.

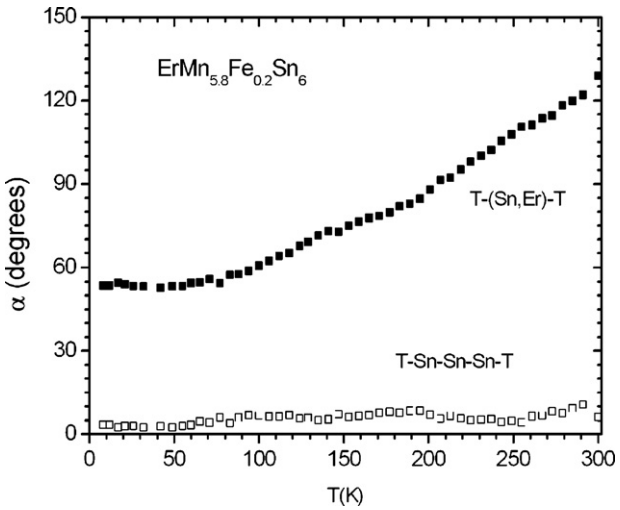

Fig. 7. Thermal variation of the angles between the T moments in the T–(Sn,Er)–T and T–Sn–Sn–Sn–T slabs in $ErMn_{5.8}Fe_{0.2}Sn_6$.

Table 3
Refined parameters of $ErMn_{5.6}Fe_{0.4}Sn_6$ at 300, 55 and 2 K.

	300 K	55 K	2 K
a (Å)	5.505(1)	5.462(1)	5.458(1)
c (Å)	8.991(2)	8.932(2)	8.929(2)
z_{Fe}	0.237(2)	0.243(1)	0.243(1)
z_{Sn}	0.333(2)	0.334(1)	0.334(1)
$m_{Fe}[m_{Mn}]$	0.084[0.916](4)	0.084[0.916]	0.084[0.916]
Helimagnetic 1			
μ_{T1} (μ_B)	–	2.00(3)	1.59(3)
θ_{Er1} (°)	–	6.84(8)	6.37(7)
θ_{T1}(°)	–	0	0
ϕ_{T1}(°)	–	194(1)	192.2(6)
q_{z1} (r.l.u.)	–	0.2070(2)	0.1695(2)
Helimagnetic 2			
μ_{T2} (μ_B)	–	1.22(7)	1.60(4)
θ_{Er1} (°)	–	2.98(20)	6.16(9)
θ_{T2} (°)	–	90	90
ϕ_{T2} (°)	–	204(2)	198.6(9)
q_{z2} (r.l.u.)	–	0.2467(9)	0.2510(3)
Commensurate			
μ_T (μ_B)	1.83(11)	0.24(2)	–
θ_T (°)	67(4)	90	–
$\mu_{T\,total}$ (μ_B)	1.83(11)	2.35(5)	2.25(5)
$\mu_{Er\,total}$ (μ_B)	0	7.46(15)	8.86(11)
R_{Bragg}, R_f	5.09; 5.74	3.04; 2.82	3.22; 2.91
R_{magn}	–;–; 8.13	3.6; 4.1; 21.1	5.3; 3.9; –
R_{wp}, R_{exp}, χ^2	13.7; 1.09; 158	9.3; 3.2; 8.5	9.0; 1.1; 65.3

The magnetic structures have been refined at the intermediate temperature T = 55 K from the data of a short duration pattern. The results are given in Table 3 and the observed and calculated patterns are displayed in Fig. 8. The refined parameters are close to those refined at 2 K.

5.2. Neutron diffraction study of $ErMn_{5.4}Fe_{0.6}Sn_6$

The pattern recorded at 300 K is characterized by the typical lines of the AF2 magnetic structure (Fig. 5b) as in the previous compound and has been refined in the same way. The results are gathered in Table 4 and the observed and calculated patterns are displayed in Fig. 11.

The pattern recorded at 2 K is characterized by one set of satellite lines and this kind of patterns, contrary to the previous compound, takes place abruptly around $T \approx 55$ K (Fig. 12). Moreover, the lines corresponding to the AF2 remains though there are much weaker than those measured at 300 K. The refinements have been undertaken firstly considering a mixture of one helimagnetic structure and the remaining AF2 structure. In the final refinements, a second helimagnetic structure has been also considered to account for the asymmetrical shape of the magnetic peaks. The results of the refinements are gathered in Table 4. The calculation of the angles between the moments in the two slabs (α = 11° and 79° for T–Sn–Sn–Sn–T and T–(Er,Sn)–T slabs respectively) still shows that the T–Sn–Sn–Sn–T is almost ferromagnetic.

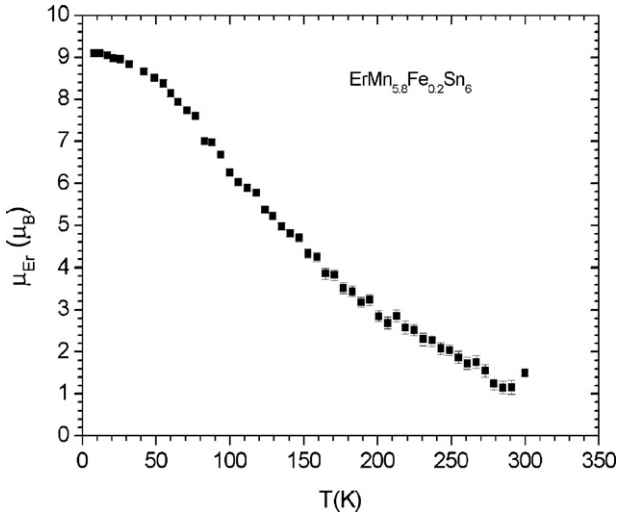

Fig. 8. Thermal variation of the Er moment in $ErMn_{5.8}Fe_{0.2}Sn_6$.

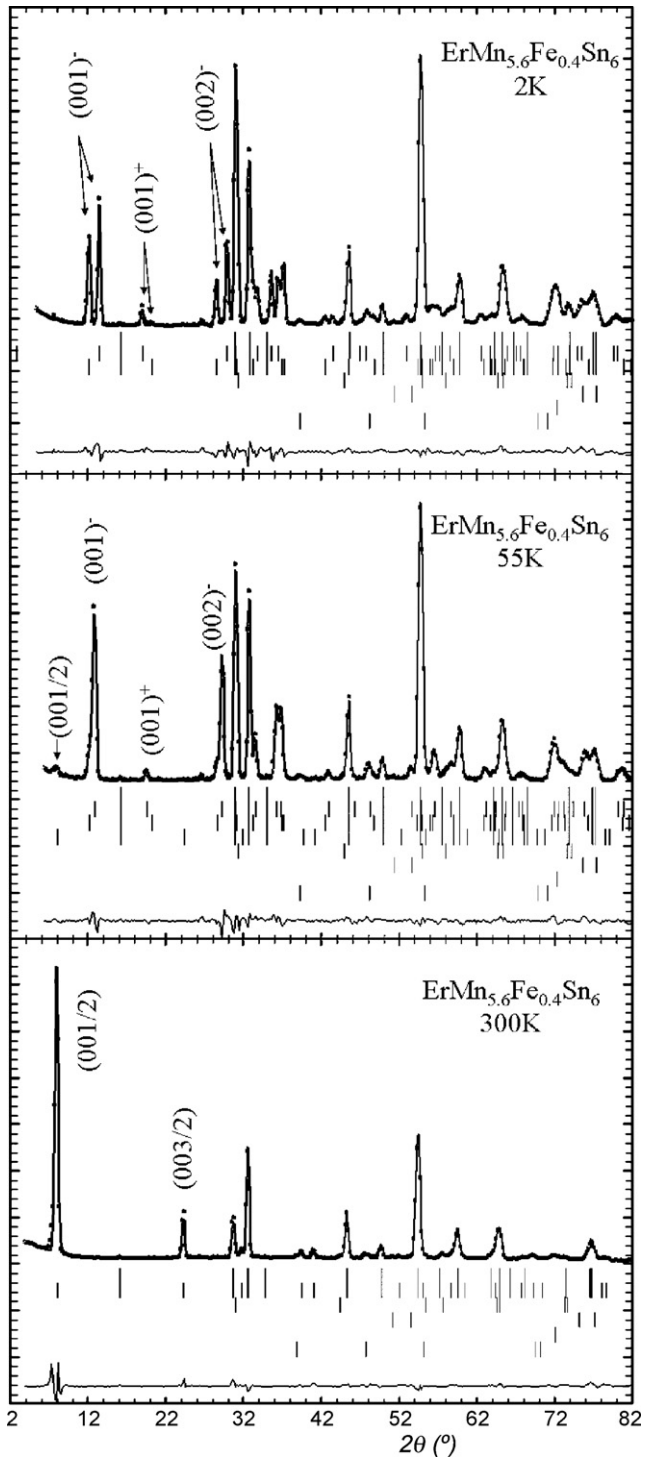

Fig. 9. Observed and calculated neutron diffraction patterns of $ErMn_{5.6}Fe_{0.4}Sn_6$ at 300, 55 and 2 K (extra lines; from bottom to top: Ni_2In-type $T_{2-x}Sn$; sample holder; elemental tin; $CuAl_2$-type TSn_2).

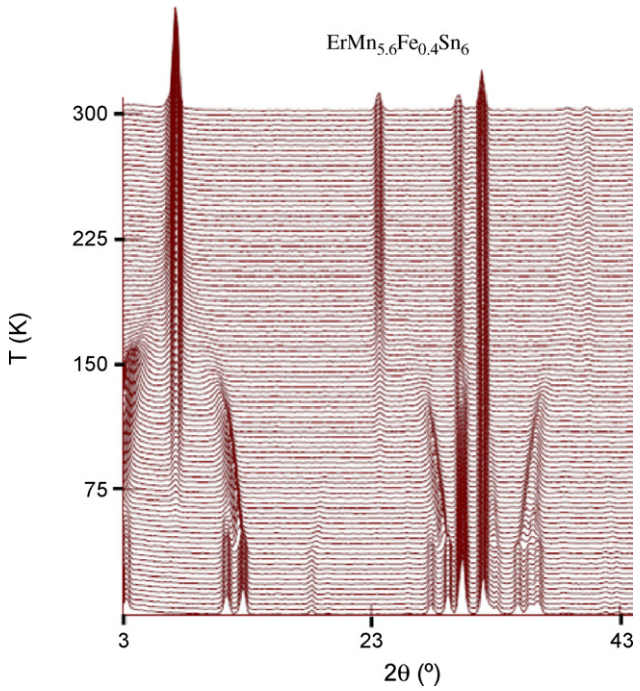

Fig. 10. Partial neutron thermogram of $ErMn_{5.6}Fe_{0.4}Sn_6$ recorded between 2 and 300 K.

5.3. Neutron diffraction study of $ErMn_{5.2}Fe_{0.8}Sn_6$

The pattern recorded at 300 K also displays the typical lines of the AF2 magnetic structure as in the previous compound and has been refined in the same way. The results are gathered in Table 5 and the observed and calculated patterns are displayed in Fig. 13.

The pattern recorded at 2 K displays, besides the remaining lines of the AF2 structure, particular features never observed in RMn_6X_6 compounds. One still observes the $(1\,0\,1)^-$, $(1\,0\,1)^+$ and $(1\,0\,2)^-$ satellites almost at the same angle as in the previous com-

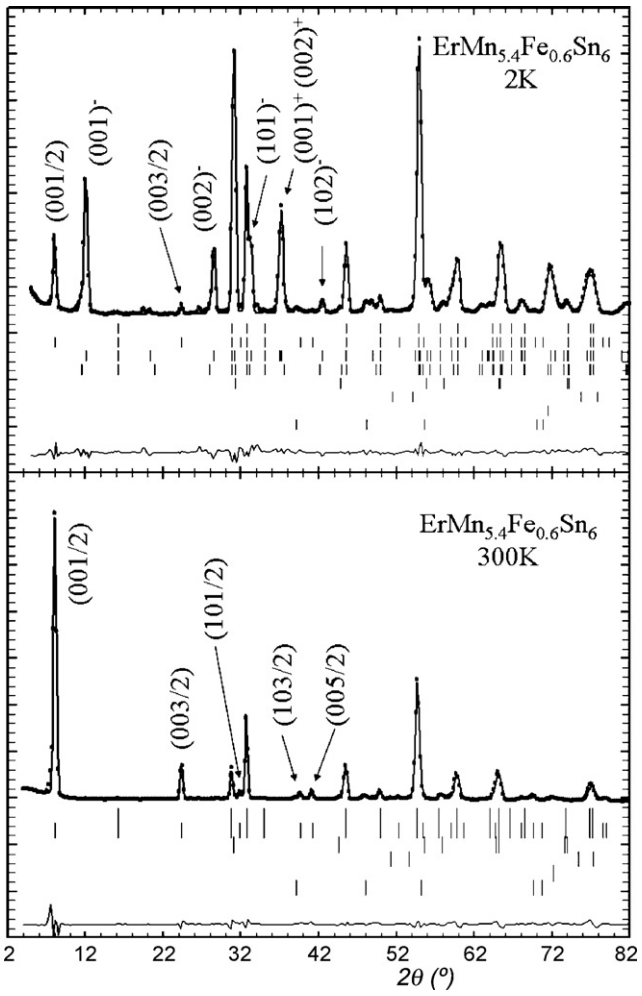

Fig. 11. Observed and calculated neutron diffraction patterns of $ErMn_{5.4}Fe_{0.6}Sn_6$ at 300 and 2 K (extra lines; from bottom to top: Ni_2In-type $T_{2-x}Sn$; sample holder; elemental tin; $CuAl_2$-type TSn_2).

Table 4
Refined parameters of $ErMn_{5.4}Fe_{0.6}Sn_6$ at 300 and 2 K.

	300 K	2 K
a (Å)	5.500(1)	5.485(1)
c (Å)	8.989(2)	8.973(2)
z_{Fe}	0.245(2)	0.245(2)
z_{Sn}	0.332(2)	0.332(1)
$m_{Fe}[m_{Mn}]$	0.124[0.876](4)	0.124[0.876]
Commensurate		
μ_T (μ_B)	1.75(9)	0.63(2)
θ_T (°)	90	90
Helimagnetic 1		
μ_{T1} (μ_B)	–	1.98(4)
θ_{Er1} (°)	–	7.96(9)
θ_{T1} (°)	–	90
ϕ_{T1} (°)	–	197.5(7)
q_{z1} (r.l.u.)	–	0.2516(3)
Helimagnetic 2		
μ_{T2} (μ_B)	–	0.67(10)
θ_{Er2} (°)	–	2.32(32)
θ_{T2} (°)	–	90
ϕ_{T2} (°)	–	206(5)
q_{z2} (r.l.u.)	–	0.2874(18)
$\mu_{T\,total}$ (μ_B)	1.75(9)	2.18(8)
$\mu_{Er\,total}$ (μ_B)	0	8.29(18)
R_{Bragg}, R_f	3.36; 4.49	2.48; 2.62
R_{magn}	4.6; –; –	9.0; 5.4; 9.3
R_{wp}, R_{exp}, χ^2	13.9; 1.2; 139	9.5; 1.1; 74.3

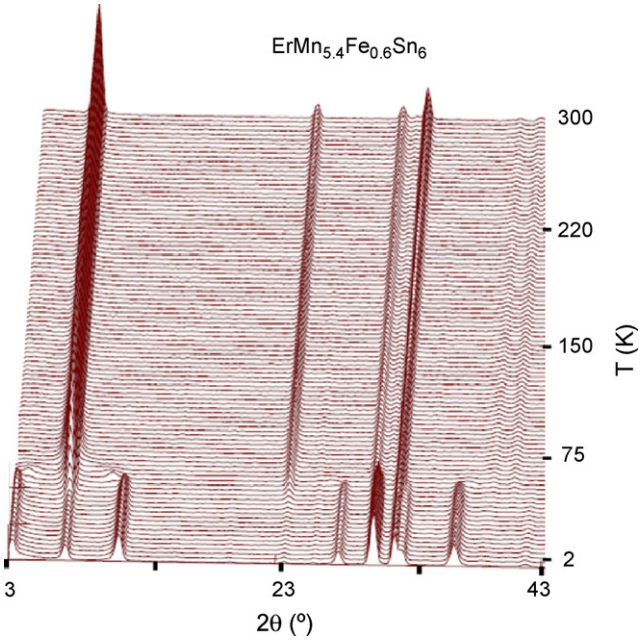

Fig. 12. Partial neutron thermogram of $ErMn_{5.4}Fe_{0.6}Sn_4Sn_6$ recorded between 2 and 300 K.

Table 5
Refined parameters of $ErMn_{5.2}Fe_{0.8}Sn_6$ at 300 and 2 K[a].

	300 K	2 K
a (Å)	5.489(1)	5.470(2)
c (Å)	8.988(2)	8.962(2)
z_{Fe}	0.245(1)	0.242(2)
z_{Sn}	0.340(2)	0.343(3)
$m_{Fe}[m_{Mn}]$	0.136[0.864](4)	0.136[0.864]
Commensurate		
μ_{T1} (μ_B)	1.81(9)	1.90(15)
θ_{T1} (°)	90	90
Sine-modulated		
$A(q)_{T2}$	–	1.62(16)
μ_{mT2} (μ_B)	–	1.14(13)
$A(q)_{Er2}$	–	11.12(27)
μ_{mEr2} (μ_B)	–	7.86 (21)
θ (°)	–	0
ϕ_{T2}(°)	–	−16(6)
q_{z2} (r.l.u.)	–	0.2574(15)
$\mu_{T\ total}$ (μ_B)	1.81	2.29(19)
$\mu_{Er\ total}$ (μ_B)	0	7.86(21)
R_{Bragg}, R_f	2.03; 2.89	5.50; 4.82
R_{magn}	7.42; –	7.21; 7.96
R_{wp}, R_{exp}, χ^2	13.5; 1.2; 125	18.6; 0.8; 512

[a] The mean magnetic moments in the sine-modulated structure μ_{mi} are calculated from the amplitudes $A(q)_i$ with the relation $\mu_m = A(q)2^{-1/2}$.

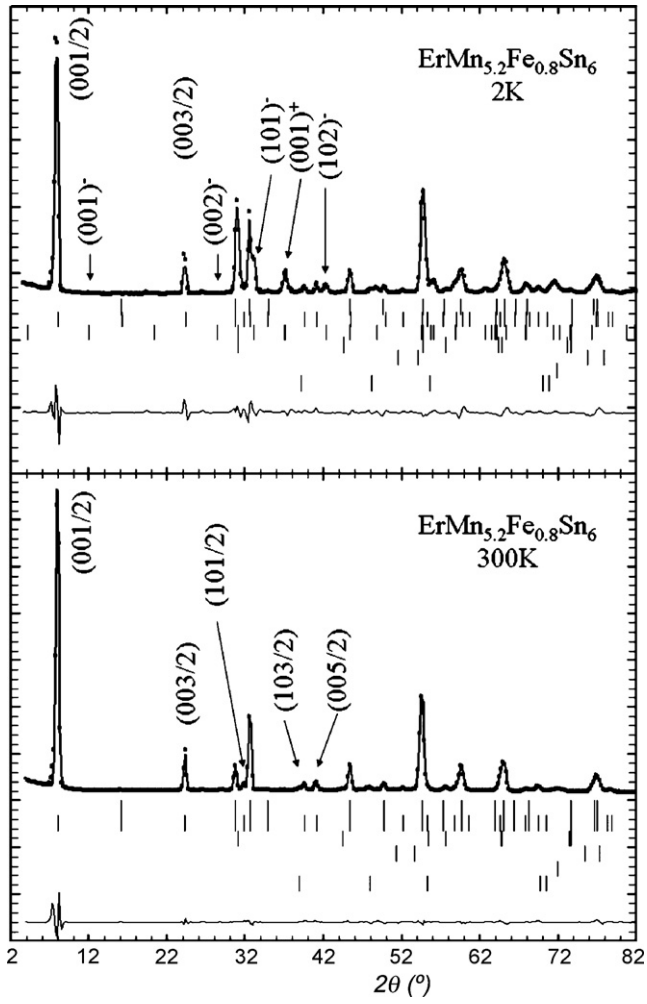

Fig. 13. Observed and calculated neutron diffraction patterns of $ErMn_{5.2}Fe_{0.8}Sn_6$ at 300 and 2 K (extra lines; from bottom to top: Ni_2In-type $T_{2-x}Sn$; sample holder; elemental tin; $CuAl_2$-type TSn_2).

Table 6
Refined parameters of $ErMn_5FeSn_6$ at 300 and 2 K[a].

	300 K	2 K
a (Å)	5.489(1)	5.462(1)
c (Å)	8.980(2)	8.955(2)
z_{Fe}	0.249(1)	0.249(2)
z_{Sn}	0.334(2)	0.335(2)
$m_{Fe}[m_{Mn}]$	0.192[0.808](4)	0.192[0.808]
Commensurate		
μ_{T1} (μ_B)	1.89(10)	2.01(13)
θ_T (°)	90	90
Ferromagnetic		
μ_{Er1} (μ_B)	0	2.80(16)
θ_{Er1} (°)	–	0
Sine-modulated		
$A(q)_{T2}$	–	1.77(13)
μ_{mT2} (μ_B)	–	1.25(10)
$A(q)_{Er2}$	–	10.32(19)
μ_{mEr2} (μ_B)	–	7.30(13)
θ (°)	–	0
ϕ_{T2} (°)	–	−12(4)
q_{z2} (r.l.u.)	–	0.256(1)
$\mu_{T\ total}$ (μ_B)	1.89	2.37
$\mu_{Er\ total}$ (μ_B)	–	7.82
R_{Bragg}, R_f	4.34;5.10	3.23; 3.31
R_{magn}	6.03; –; –	5.10;4.55;6.70
R_{wp}, R_{exp}, χ^2	12.3; 1.28; 92.7	13.9; 1.03; 184

[a] The mean magnetic moments in the sine-modulated structure μ_{mi} are calculated from the amplitudes $A(q)_i$ with the relation $\mu_m = A(q)2^{-1/2}$.

pound $ErMn_{5.4}Fe_{0.6}Sn_6$ but the $(0\,0\,l)^{\pm}$ satellites are missing. Such an observation is compatible with a sine-wave modulated structure (SM) with moments aligned along the direction of the propagating vector $Q = (0, 0, 0.2574)$. The refinements have been undertaken considering (Mn,Fe) and Er moments aligned along the [0 0 1] direction ($\theta = 0°$). The refined parameters were the magnitude of the (Mn,Fe) and Er moments and a phase ϕ_T and $-\phi_T$ respectively for the moments of (Mn,Fe) sites at $z \approx 1/4$ and $z \approx 3/4$. Since it remains the lines of the AF2 structure, a mixture of the AF2 structure and of the sine-wave modulated structure has been considered. The results are gathered in Table 5 and the observed and calculated patterns are displayed in Fig. 13.

A representation of the sine-wave modulated structure is given in Fig. 5d. The Er and (Mn,Fe) moments display a modulation with a wavelength close to four chemical cells. Therefore, there is a succession of Er moments alternately up, weak, down, weak. The (MnFe) moments in each site at $z \approx 1/4$ and $z \approx 3/4$ follow the same sequence but the phase angle is refined to a value which keeps the ferromagnetic arrangement in the T–Sn–Sn–Sn–T slab. A modulation of the Mn moment magnitude has been still observed in the $ZrMn_6Sn_{6-x}Ga_x$ solid solution [18]. The value of the q_z component of the propagating vector being close to 1/4, higher order harmonics should be located at Bragg angles close to those related to the first harmonics. Therefore, we cannot exclude a possible square-wave modulated structure.

5.4. Neutron diffraction study of $ErMn_5FeSn_6$

The evolution of the neutron diffraction patterns of the compound $ErMn_5FeSn_6$ is close to that observed in the previous compound $ErMn_{5.2}Fe_{0.8}Sn_6$. The pattern recorded at 300 K displays the typical line of the AF2 structure which has been refined in the same way (Fig. 14). The results are gathered in Table 6.

The pattern recorded at 2 K is also compatible with an additional sine-wave modulated structure, the corresponding lines beginning to grow below 40 K. The only difference with the previous compound is the occurrence of the weak (1 0 1) line below 31 K which

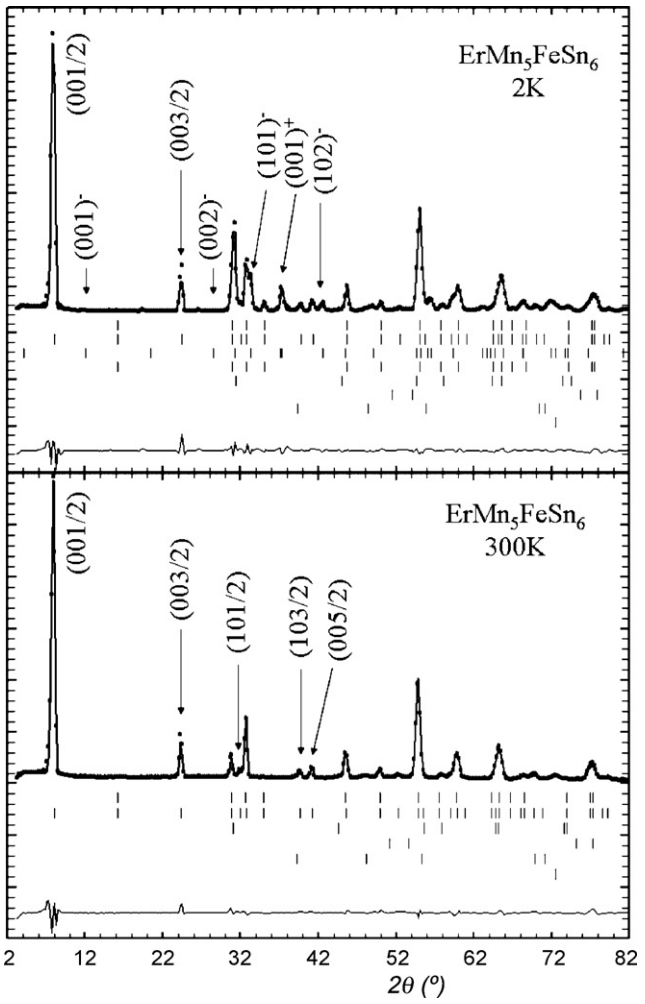

Fig. 14. Observed and calculated neutron diffraction patterns of $ErMn_5FeSn_6$ at 300 and 2 K (extra lines; from bottom to top: sample holder; Ni_2In-type $T_{2-x}Sn$; elemental tin; $CuAl_2$-type TSn_2).

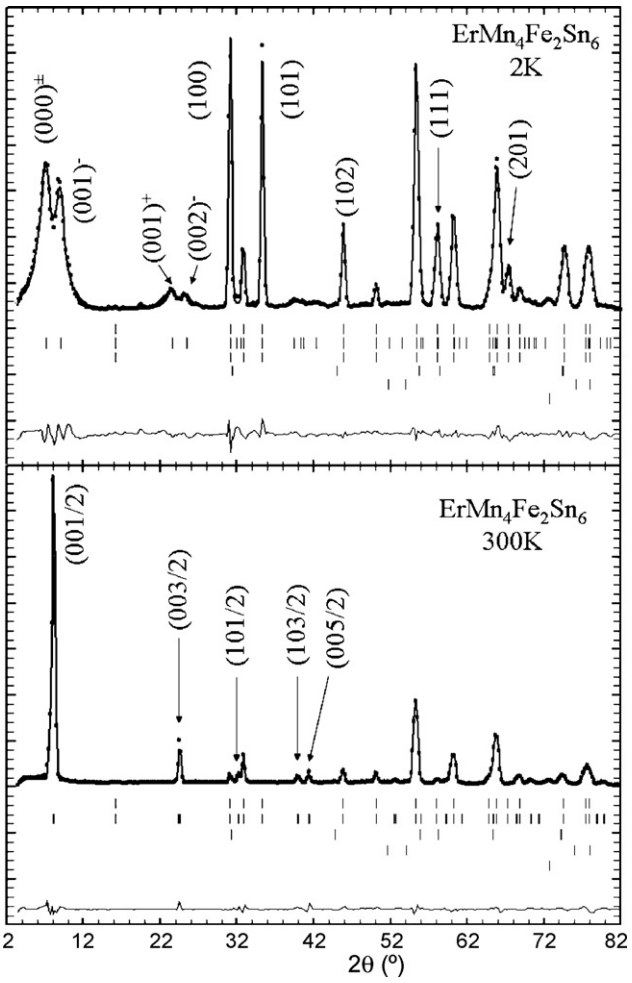

Fig. 15. Observed and calculated neutron diffraction patterns of $ErMn_4Fe_2Sn_6$ at 300 and 2 K (extra lines; from bottom to top: sample holder; elemental tin; $CuAl_2$-type TSn_2).

might indicate the onset of a ferromagnetic component onto the Er sublattice. The refinements have therefore undertaken considering a mixture of the remaining AF2 structure of the (Mn,Fe) sublattice, a modulated structure and a ferromagnetic arrangement of the Er sublattice. The results are given in Table 6.

5.5. Neutron diffraction study of $ErMn_4Fe_2Sn_6$

The pattern recorded at 300 K (Fig. 15) still displays the typical lines of the AF2 structure which has been refined in the same way (Table 7).

Below 170 K, shoulders appear at each side of the (0, 0, 1/2) line which begins to decrease. Below 50 K, the (0, 0, 1/2) line cannot be distinguished from the two wide and intense satellites $(0\,0\,1)^-$ and $(0\,0\,1)^+$ which have grown. At this temperature, it is observed the growth of the nuclear lines (1 0 0), (1 0 1), (1 0 2), (1 1 1) and (2 0 1) which had very weak intensities in the pattern recorded at 300 K. These lines are typical of a ferromagnetic ordering of the Er sublattice. The missing (0 0 1) line and the absence of variation of the intensities of the (0 0 2) and (0 0 3) lines indicate that the moment is aligned along the [0 0 1] direction. The refinements have been done considering a mixture of a helimagnetic structure and of a ferromagnetic structure. For the helimagnetic structure, the classical parameters have been firstly refined. These preliminary refinements have shown that the erbium moment did not get a

Table 7
Refined parameters of $ErMn_4Fe_2Sn_6$ at 300 and 2 K.

	300 K	2 K
a (Å)	5.469(1)	5.450(1)
c (Å)	8.968(2)	8.944(1)
z_{Fe}	0.246	0.246
z_{Sn}	0.338(1)	0.338(1)
$m_{Fe}[m_{Mn}]$	0.352[0.648](4)	0.352[0.648](4)
Helimagnetic 1		
μ_{T1} (μ_B)	–	2.31(2)
θ_{T1} (°)	–	90
ϕ_{T1} (°)	–	49.6(8)
q_{z1} (r.l.u.)	–	0.4419(6)
Commensurate		
μ_T (μ_B)	1.78(2)	0.60(3)
θ_T (°)	90	0
μ_{Er} (μ_B)	–	8.76(8)
θ_{Er} (°)	–	0
$\mu_{T\,total}$ (μ_B)	1.78	2.39
$\mu_{Er\,total}$ (μ_B)	0	8.76
R_{Bragg}, R_f	5.02; 4.58	3.45; 2.48
R_{magn}	–; 4.98	4.19; 3.98
R_{wp}, R_{exp}, χ^2	10.3; 1.74; 35.2	8.38; 1.08; 60.1

significant value. In the final refinement, only a moment onto the (Mn,Fe) sublattice has been considered. The refined phase angle leads to an angle between the moment in the T–(Sn,Er)–T slab close to 178° and to an angle close to 18° in the T–Sn–Sn–Sn–T slab. The T–(Sn,Er)–T slab is therefore almost antiferromagnetic, a feature which should explain the absence of moment on the Er sublattice.

For the ferromagnetic structure, the only Er moment has been firstly refined. In a second step, a small ferromagnetic component ($0.60\mu_B$) of the (Mn,Fe) sublattice has been added yielding a slight improvement of the corresponding reliability factor. The results are gathered in Table 7 and the observed and calculated patterns are displayed in Fig. 15. A representation of the helimagnetic arrangement is given in Fig. 6b and the ferrimagnetic structure is depicted in Fig. 5e.

5.6. Neutron diffraction study of $ErMn_3Fe_3Sn_6$

The patterns of this compounds are all characterized by the presence of the satellites $(0\,0\,1)^-$ and $(0\,0\,1)^+$ thus indicating the stability of an incommensurate structure in the whole investigated temperature range (Fig. 16). Like in the previous compound, the intensity of these satellites is large and significantly larger than the intensity of the $(0\,0\,2)^-$ and $(0\,0\,2)^+$ lines, in contrast with the patterns of the iron-poor compound $ErMn_{5.8}Fe_{0.2}Sn_6$.

It also observed that the (0 0 1) line displays an intensity which is larger than the pure nuclear contribution. This feature may arise from an antiferromagnetic AF1 ordering of the T sublattice (see Section 5.7) or from a partial order of the Mn and Fe atoms on the successive (0 0 1) planes. Since this latter model does not well fit the other nuclear intensities, we have considered a small contribution arising from the AF1 arrangement.

There are some other phenomena taking place upon cooling. Below $T \approx 40$ K, it is observed a sudden increase of the $(1\,0\,0)^{\pm}$ and $(1\,0\,1)^+$ lines associated with a small decrease of the $(0\,0\,1)^{+\text{ and }-}$ lines (Fig. 17). The $(1\,0\,0)^{\pm}$ and $(1\,0\,1)^+$ lines decrease again below $T \approx 25$ K whereas the (1 0 1) line increases. These features may be interpreted as follows: there is an intermediate temperature range between 40 and 25 K where a modification of the helimagnetic structure takes place and this modification disappears when the ferromagnetic structure occurs.

The pattern recorded at 300 K has been firstly analyzed considering a mixture of one helimagnetic structure and one antiferromagnetic structure AF1 to account for the intensity of the (0 0 1) line. The helimagnetic structure is defined as in the previous compound $ErMn_4Fe_2Sn_6$ with a non-zero moment only on the (Mn,Fe) sublattice. In a second step, another helimagnetic structure with slightly different propagating vector has been added to account for the asymmetrical shape of the satellites. The results of the final refinements are given in Table 8. The antiferromagnetic structure AF1 is characterized by a very small moment. The phase angles for the helimagnetic structure give rise to an almost antiparallel arrangement in the T–(Er,Sn)–T slab like in the previous compound.

The phenomenon taking place between 40 and 24 K should be related to that observed in $ErMn_5FeSn_6$. In this compound, the growth of the $(1\,0\,1)^+$ satellite has been attributed to the apparition of a sine-wave modulated structure. Therefore, the same kind of magnetic structure has been refined in this temperature range together with the remaining antiferromagnetic structure AF1. The second helimagnetic structure has been also kept to account for the anisotropic shape of the satellites. The results of the refinements are gathered in Table 8. The sine-wave modulated structure is characterized by a rather small value of its reliability factor ($R = 6.1\%$) and the main part of the (Mn,Fe) moment is concentrated in this structure. The value of the propagating vector component is close to 1/6 thus suggesting that the structure might

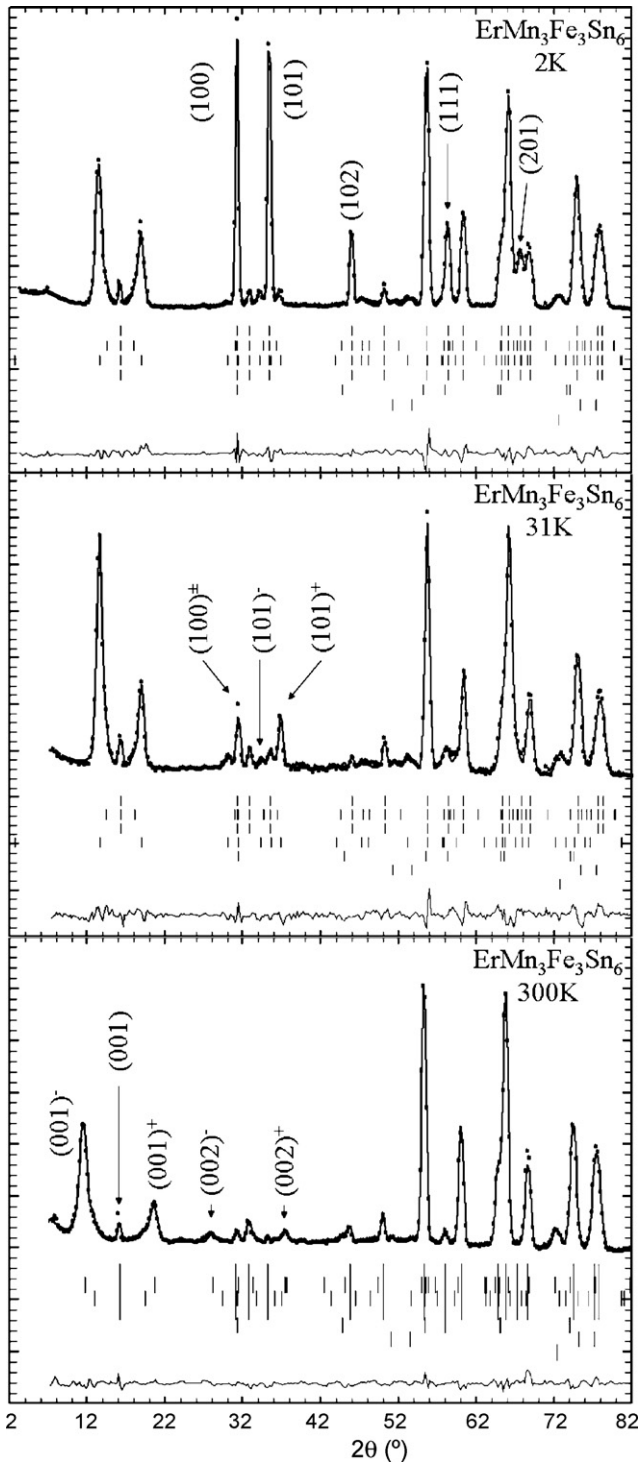

Fig. 16. Observed and calculated neutron diffraction patterns of $ErMn_3Fe_3Sn_6$ at 300, 31 and 2 K (extra lines; from bottom to top: sample holder; elemental tin; $CuAl_2$-type TSn_2).

be described into a commensurate model with a six-time larger cell.

Below 24 K, the $(1\,0\,0)^{\pm}$ and $(1\,0\,1)^+$ lines decrease and the satellites $(0\,0\,1)^{+\text{ and }-}$ slightly increase. It looks like the helimagnetic structure becomes again similar to the high temperature one. Simultaneously, the (1 0 0) and (1 0 1) lines increase giving evidence of the stabilisation of a ferromagnetic structure for the Er sublattice. In this compound, it looks like the ordering of the erbium moment takes place in two steps, firstly a sine-wave modulated structure and

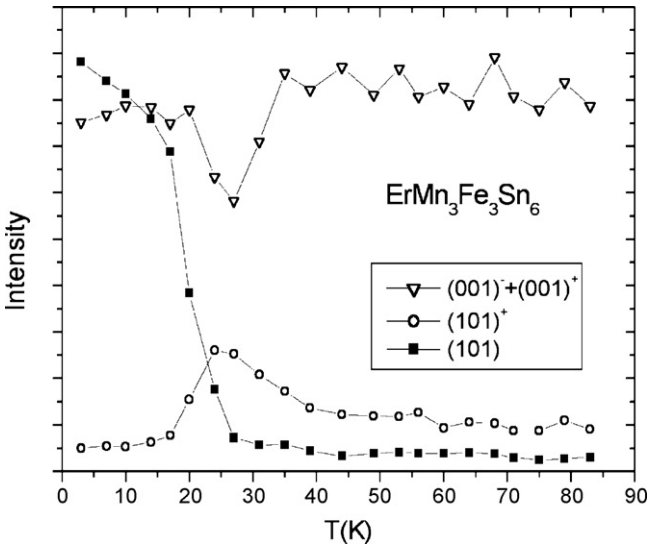

Fig. 17. Thermal variation of some characteristic diffracted intensities of $ErMn_3Fe_3Sn_6$.

then a ferromagnetic one. The refinements have been undertaken considering the two helimagnetic structures described for the 300 K pattern and a commensurate structure including the ferromagnetic Er structure and the antiferromagnetic structure AF1 for the (Mn,Fe) sublattice. In this structure a tilting of the (Mn,Fe) moments has been allowed to account for an eventual antiferromagnetic coupling

Table 8
Refined parameters of $ErMn_3Fe_3Sn_6$ at 300, 31 and 2 K[a].

	300 K	31 K	2 K
a (Å)	5.439(1)	5.420(1)	5.416(1)
c (Å)	8.949(2)	8.932(2)	8.929(2)
z_{Fe}	0.248(1)	0.245(2)	0.247(2)
z_{Sn}	0.340(1)	0.342(2)	0.347(2)
$m_{Fe}[m_{Mn}]$	0.504[0.496](4)	0.504[0.496]	0.504[0.496]
Helimagnetic 1			
μ_{T1} (μ_B)	1.80(5)	–	2.22(7)
θ_{T1} (°)	56(1)	–	58(1)
ϕ_{T1} (°)	52(1)	–	71(3)
q_{z1} (r.l.u.)	0.275(1)	–	0.1642(6)
Helimagnetic 2			
μ_{T2} (μ_B)	0.82(7)	0.58(9)	0.84(8)
θ_{T2} (°)	52(1)	18(3)	58(1)
ϕ_{T2} (°)	55(6)	79(38)	102 (22)
q_{z2} (r.l.u.)	0.200(4)	0.112(4)	0.106(3)
Commensurate			
μ_{T3} (μ_B)	0.31(2)	0.37(3)	0.67(3)
θ_{T3} (°)	90	90	36(2)
μ_{Er3} (μ_B)	–	–	8.27(8)
θ_{Er} (°)	–	–	0
Sine-modulated			
$A(q)_{T4}$ (μ_B)	–	2.98(13)	–
μ_{mT4} (μ_B)	–	2.11(9)	–
θ_{T4} (°)	–	128(3)	–
ϕ_{T4} (°)	–	−309(2)	–
$A(q)_{Er4}$	–	4.25(27)	–
μ_{mEr4} (μ_B)	–	3.00(21)	–
θ_{Er4} (°)	–	−21(2)	–
q_{z4} (r.l.u.)	–	0.1647(5)	–
$\mu_{T\,total}$ (μ_B)	1.95	2.22	2.45
$\mu_{Er\,total}$ (μ_B)	0	4.25	8.27
R_{Bragg}, R_f	3.01; 2.64	4.24; 2.73	2.50; 2.00
R_{magn}	7.7; 8.9; 17.2; –	–; 11.3; 15.5; 6.1	6.53; 12.2; 1.39; –
R_{wp}, R_{exp}, χ^2	8.39; 1.84; 20.6	11.3; 4.81; 5.55	8.47; 1.14; 54.8

[a] The mean magnetic moments in the sine-modulated structure μ_{mi} are calculated from the amplitudes $A(q)_i$ with the relation $\mu_m = A(q)2^{-1/2}$.

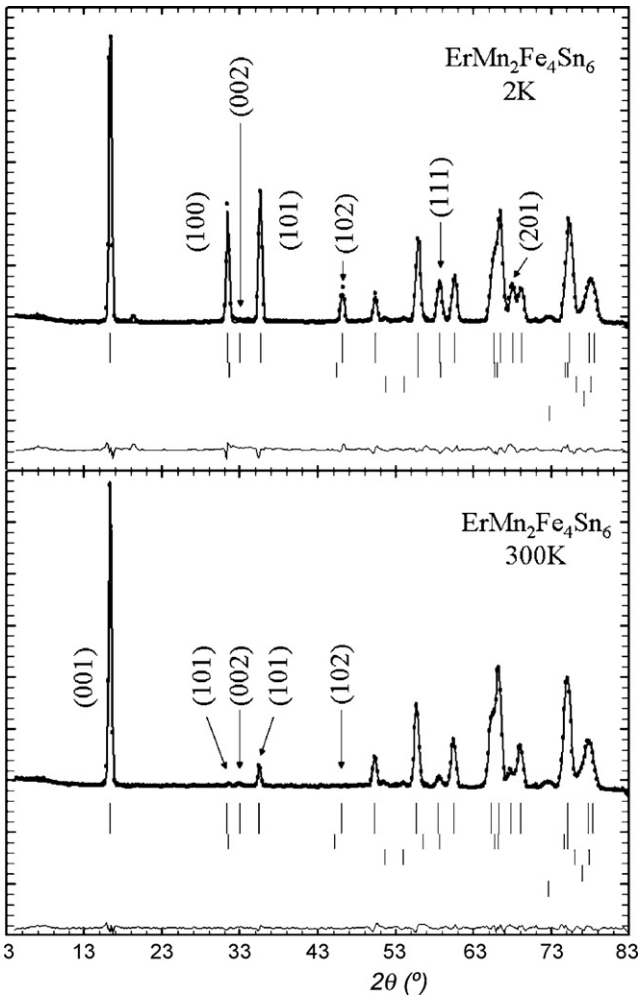

Fig. 18. Observed and calculated neutron diffraction patterns of $ErMn_2Fe_4Sn_6$ at 300 and 2 K (extra lines; from bottom to top: sample holder; BCC (T,Sn) alloy, elemental tin; $CuAl_2$-type TSn_2).

with the ferromagnetic Er sublattice. The results of the refinement are gathered in Table 8. The commensurate structure is characterized by a canting angle of 36°. The in-plane antiferromagnetic component of the (Mn,Fe) sublattice is therefore 0.39μ_B and the axial component opposite to the erbium moment is 0.54μ_B.

5.7. Neutron diffraction study of $ErMn_2Fe_4Sn_6$

The room temperature pattern (Fig. 18) is mainly characterized by the large intensity of the (0 0 1) and (1 0 1) lines which are characteristic of the AF1 magnetic structure often observed for MFe_6X_6 compounds. The presence of the (0 0 1) line indicates that the moments are not aligned along [0 0 1]. The refinements have been undertaken taking into account these preliminary remarks. The best refinements lead to put the Mn(Fe) moments in the (0 0 1) plane. The results are gathered in Table 9 and the observed and calculated patterns are presented in Fig. 18. The magnetic structure is depicted in Fig. 5f.

Below 26 K (Fig. 18), it is observed a considerable growth of the (1 0 0) and (1 0 1) lines. These lines are characteristic of the ferromagnetic ordering of the Er sublattice as observed in previous sections. The absence of contribution of the Er magnetic moments on the (0 0 l) lines indicates that the Er moments are aligned along the c-axis. The refinements have been firstly done considering a ferromagnetic ordering of Er along [0 0 1] and the remaining AF1

Table 9
Refined parameters of $ErMn_2Fe_4Sn_6$ at 300 and 2 K.

	300 K	2 K
a (Å)	5.425(1)	5.404(1)
c (Å)	8.944(2)	8.918(2)
z_{Fe}	0.251(2)	0.255(2)
z_{Sn}	0.340(2)	0.341(2)
$m_{Fe}[m_{Mn}]$	0.680[0.320](4)	0.680[0.320]
μ_T (μ_B)	1.89(3)	2.13(4)
θ_T (°)	90	80(2)
μ_{Er} (μ_B)	–	8.49(12)
θ_{Er} (°)	–	0
R_{Bragg}, R_f	5.69, 3.57	4.09, 2.94
R_{magn}	2.65	3.01
R_{wp}, R_{exp}, χ^2	11.5; 1.81; 40.6	10.8; 1.38; 61.2

ordering of the transition metal sublattice in the (0 0 1) plane yielding a residual magnetic factor of 3.5% with some slight discrepancies on the (1 0 0) and (1 0 1) lines. A canting of the Mn(Fe) moments have been taken into account considering that a part of the Mn(Fe) moment couples antiferromagnetically with the ferromagnetic Er sublattice. The refinements converge for a canting angle of 10(1)° with slightly weaker residual factors (Table 9). A representation of the corresponding magnetic structure is given in Fig. 5g.

6. Discussion

The study of the $ErMn_{6-x}Fe_xSn_6$ solid solutions makes evidence of new magnetic arrangements which had never been observed in $HfFe_6Ge_6$-type stannides.

The first one is the sine-wave modulated structure observed for $ErMn_{5.2}Fe_{0.8}Sn_6$ and $ErMn_5FeSn_6$ with a propagating vector close to $Q=(0, 0, 1/4)$ and for $ErMn_3Fe_3Sn_6$ with a propagating vector close to $Q=(0, 0, 1/6)$. The stabilisation of this kind of magnetic structure might be the result of the combination of two particular features: an easy axis anisotropy for the Er sublattice and a relatively weak Er–(Mn,Fe) magnetic coupling not sufficient to align the T=(Mn,Fe) moments. Up to now, only the terbium moment displayed an easy axis in the ternary stannides and the strong Tb–Mn interaction was able to align the Mn moments leading to an easy axis ferrimagnetic structure. On another hand, the easy plane anisotropy of Er and Tm moments in ternary stannides [5,6] and the weak Er(Tm)–Mn interaction were fully satisfied by the stabilisation of the in-plane helimagnetic structure for $TmMn_6Sn_6$ and for $ErMn_6Sn_6$ above 62 K. As the substitution of Fe for Mn in the $ErMn_{6-x}Fe_xSn_6$ solid solutions seems to change the easy direction of the erbium moments, one may assume that a sine-wave modulated structure is a convenient way to satisfy both the easy axis of the Er moment and the weak Er–T interaction.

Another new magnetic arrangement is observed in the helimagnetic structures of $ErMn_4Fe_2Sn_6$ and $ErMn_3Fe_3Sn_6$. Up to now, the helimagnetic structures observed in ternary stannides were characterized by an almost ferromagnetic Mn–Sn–Sn–Sn–Mn slab and by a more or less opened angle between the Mn moments into the Mn–(Sn,R)–Mn slab. The helimagnetic structures observed in the iron-rich compounds of the present solid solutions are characterized by an almost antiferromagnetic T–(Sn,R)–T slab and by a more or less opening of the angle between the T=(Mn,Fe) moments into the T–Sn–Sn–Sn–T slab. This structure, which is experimentally observed for the first time, should be recognized as the helimagnetic structure H2 predicted by Rosenfeld et al. [19] during their theoretical work on the magnetic properties of RMn_6X_6 compounds. According to their model of double flat spiral based on the two nearest J_1 (within the Mn–Sn–Sn–Sn–Mn slab) and J_2 (within the Mn–(Sn,R)–Mn slab) and the next-nearest J_3 interactions, two different helimagnetic structures can be distinguished. Both are stable for a product $J_1.J_2.J_3<0$. In addition, the classical helimagnetic structure H1 of the RMn_6X_6 compounds is stable for $J_1.J_3<0$ and gives rise to large intensity for the satellites $(0\,0\,l)^{+-}$ with l even while the helimagnetic structure H2 is stable for $J_1.J_3>0$ and gives rise to large intensity for the satellites $(0\,0\,l)^{+-}$ with l odd. The H2 structure may be regarded as the missing link between the AF2 (ferromagnetic T–Sn–Sn–Sn–M–T slab and antiferromagnetic T–(Sn,R)–T slab) and the AF1 structures (antiferromagnetic T–Sn–Sn–Sn–T slab and antiferromagnetic T–(Sn,R)–T slab).

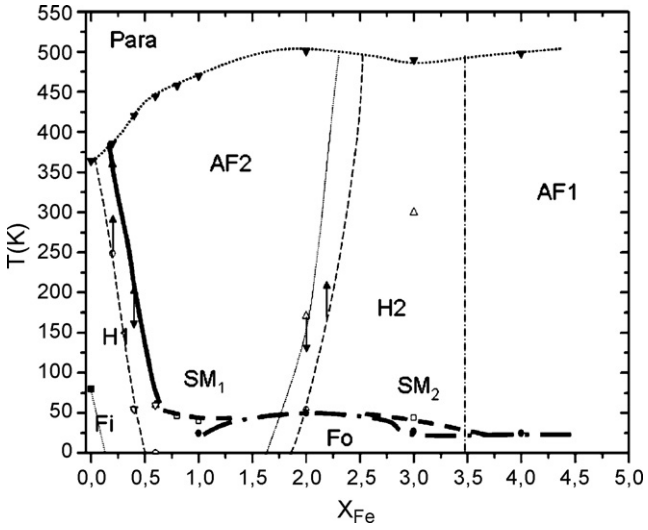

Fig. 19. Schematized x–T phase diagram of the $ErMn_{6-x}Fe_xSn_6$ compounds.

The data of the neutron diffraction and magnetic measurements enable to draw a schematic x–T magnetic phase diagram for the hexagonal compounds $ErMn_{6-x}Fe_xSn_6$ (Fig. 19). Several comments may be done.

The magnetic phases stable in the high temperature range (above $T\approx 50$ K) mainly account for the magnetic behaviour of the T=(Mn,Fe) sublattice alone. We observe four domains which are rather well correlated to the iron content with the evolution H1 → AF2 → H2 → AF1 towards the iron-rich region. This evolution might be related to the analysis of the properties of the 1-6-6 compounds undertaken by Rosenfeld et al. [19] and summarized by the stability diagram reported in Fig. 20. Obviously, the successive observed stable phases cross the stability diagram from the down-right quarter towards the up-left quarter following approximately the arrow depicted in Fig. 20.

In their work, Rosenfeld et al. [19] give expressions linking the observed characteristic angles of the helical structure (turn angle Φ and angle δ between the Mn moments belonging to the Mn–Sn–Sn–Sn–Mn slab) to the ratio J_2/J_1 and J_3/J_1. We have tried to get approximate values of these ratios using a graphical method. The results are given in Table 10.

For the helical H1 structure of $ErMn_{5.8}Fe_{0.2}Sn_6$, the observed angles lead to small values of the ratio J_2/J_1 and J_3/J_1 meaning that the value of the positive J_1 interaction is relatively large with respect to positive J_2 and negative J_3 interactions. This is in relation with the almost ferromagnetic T–Sn–Sn–Sn–T slab ($\delta=2.6°$). The corresponding energy of the H1 structure, which expression is also given in Ref. [19], is only slightly smaller than those of the ferromagnetic F structure and antiferromagnetic AF2. This observation should be related to the temperature-induced transition between the high temperature AF2 structure and the low temperature H1 structure observed for this compound. The close values between the energy of the H1 and F structures may be also related to the magnetic behaviour of the ternary stannides which become easily ferromagnetic by minor substitution of tin by gallium or indium [20].

Table 10
Refined parameters of the T sublattice and corresponding characteristic angles. Estimated J_2/J_1 and J_3/J_1 values and corresponding energy E_i of the magnetic structures (in J_1 unit) [19]. The angles δ_o and Φ_o are deduced from the refinements and the angles δ_c and Φ_c are calculated from the J_2/J_1 and J_3/J_1 values.

x	z_T	q_z (r.l.u.)	ϕ_T (°)	δ (°)	Φ (°)	$\Phi-\delta$ (°)	$\cos(\delta_o)$	$\cos(\Phi_o)$
0.2	0.245(1)	0.3752(4)	213.2(6)	2.6	135.1	132.5	0.9989	−0.7083
2.0	0.246	0.4419(6)	49.6(7)	−18.3	159.1	177.5	0.9494	−0.9342
3.0	0.247(2)	0.1642(6)	71(2)	−112	59.1	171.1	−0.3746	0.5135

x	J_2/J_1	J_3/J_1	E_H	E_F	E_{AF1}	E_{AF2}	$\cos(\delta_c)$	$\cos(\Phi_c)$
0.2	0.08	−0.0378	−1.0046	−1.0044	1.1556	−0.9956	0.9986	−0.7087
2.0	−7.5	0.4442	−7.6118	5.6116	−7.3884	−7.6116	0.9488	−0.9346
3.0	−6.0	0.5402	−6.1080	3.9196	−6.0804	−5.9196	−0.3744	0.5132

For the compounds $ErMn_4Fe_2Sn_6$ and $ErMn_3Fe_3Sn_6$, the characteristic angles lead to a large negative value for the ratio J_2/J_1 while the ratio J_3/J_1 is close to 1/2. This suggests that J_2 has decreased from the small initial positive value to a relatively large negative value while J_1 has decreased from a relatively large positive value to a small positive value. Correlatively, it is suggested that J_3 has changed from a small negative value to a small positive value. The value of the ratio J_3/J_1 is related to the relative strengths of J_1 and J_3:

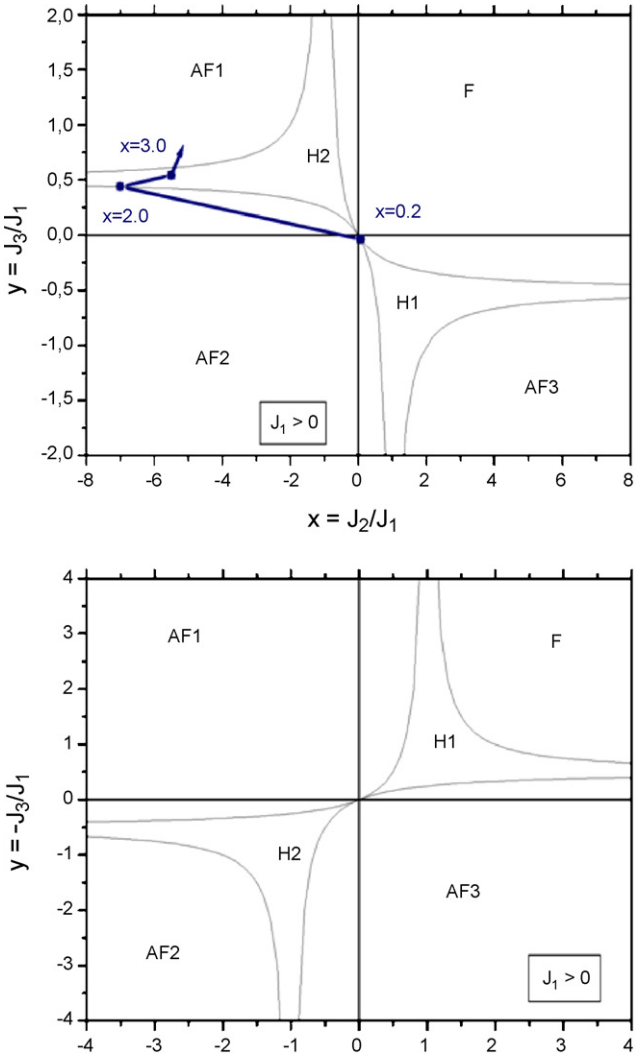

Fig. 20. Calculated magnetic phase diagram from Ref. [19] and a possible pathway for the observed evolution. (According to a correspondence with the authors, in the case $J_1 < 0$, the abscissa and ordinate have been changed in $x = -J_2/J_1$ and $y = -J_3/J_1$.)

(i) for $ErMn_4Fe_2Sn_6$, this ratio is less than 1/2 meaning that J_1 is preponderant thus accounting for an almost ferromagnetic T–Sn–Sn–Sn–T slab ($\delta = -18.3°$);
(ii) for $ErMn_3Fe_3Sn_6$, this ratio is greater than 1/2 meaning that J_3 is preponderant in relation with the smaller value of the angle Φ (59.1°).

For the following composition $ErMn_2Fe_4Sn_6$, two possible ways may be expected. Either J_3 still increases (J_1 and J_2 remaining unchanged) and the structure enters in the AF1 range in the phase diagram, or J_1 follows its decrease and becomes negative (J_3 and J_2 remaining unchanged) and the stability conditions of the AF1 structure are fulfilled ($J_1 < 0, J_2 < 0, J_3 > 0$). The high Néel temperatures of the ternary iron compounds strongly suggest this latter hypothesis. The magnetic structure observed for the compounds of intermediate composition ($0.4 < x < 1$) suggests that the pathway from the H1 range towards the H2 range goes across the AF2 range.

The bold curve in the diagram underlines the ordering temperature of the Er sublattice. Below the phases AF2, H2 and AF1, the erbium moment orders at low temperature whereas a non-zero moment is measured in the phase H1. This feature should be related to the moment arrangement in the corresponding T–(Sn,Er)–T slab: since the moments of T = (Mn,Fe) are not antiparallel in this slab, the Er site experiences a molecular field yielding an induced non-zero value of the Er moment.

The low temperature part of the diagram is rather complicated and we observe a different behaviour for nearly all the studied compounds. Starting from the compound $ErMn_6Sn_6$, previous studies have shown the existence of the ferrimagnetic phase (Fi) below 62 K [2]. There is probably a small zone of a ferrimagnetic phase (Fi) in the Mn-rich region but this phase has already disappeared in the compound $ErMn_{5.8}Fe_{0.2}Sn_6$. However, the metamagnetic behaviour of this phase (Section 4) suggests that this ferrimagnetic phase is almost stable. The existence of this phase in the ternary compound is related to the Er–Mn interaction which is strong enough to align the Mn moments. The vanishing of this phase in $ErMn_{5.8}Fe_{0.2}Sn_6$ indicates that this small amount of iron is large enough to increase the antiferromagnetic character of the T–(Sn,Er)–T slab and the phase H1 remains stable down to 2 K, the moments rotating in the (0 0 1) plane in accordance with the in-plane anisotropy of the erbium moment. The occurrence of the two well distinguished phases of H1 type at low temperature for the compound $ErMn_{5.6}Fe_{0.4}Sn_6$ is rather surprising and it looks like this compound was not homogeneous. For the compound $ErMn_{5.4}Fe_{0.6}Sn_6$, there is again one phase H1 but, this time, the moments rotate in a plane containing the c axis, thus suggesting that the anisotropy of erbium has changed. For the compound $ErMn_{5.2}Fe_{0.8}Sn_6$, it appears at low temperature a sine-wave modulated structure besides the remaining AF2 phase. It seems that, upon this iron concentration, there is a hard easy axis anisotropy direction of erbium. For the compound $ErMn_5FeSn_6$, a sine-wave modulated structure is also observed below 40 K, but a second

transition takes place below 31 K where a ferromagnetic component appears. For the other compounds $ErMn_4Fe_2Sn_6$, $ErMn_3Fe_3Sn_6$ and $ErMn_2Fe_4Sn_6$ a ferromagnetic state appears below 50, 24 and 26 K respectively. However, for an unknown reason, in the compound $ErMn_3Fe_3Sn_6$, the erbium sublattice firstly orders in an intermediate modulated structure between 40 and 24 K.

A last point concerns the Er–T interactions. It is observed for $x = 2$, 3 and 4, that the ferromagnetic ordering of the erbium sublattice is accompanied by a small tilting of the T moments yielding the apparition of a small ferromagnetic component opposite to the ferromagnetic Er sublattice. This component seems to decrease when x increases and the extrapolated value for the hypothetic hexagonal ternary iron compound should be very weak. This evolution is probably related to the strong AF character of the Fe sublattice. It may explain why an independent ordering of the iron and lanthanide sublattices has been assumed in previous studies of the orthorhombic ternary iron compounds [8–11]. The small Er–T coupling in the present compounds might explain the higher ordering temperature of the erbium moment in these compounds with respect to the ordering temperature measured in the ternary compound $ErFe_6Sn_6$ ($T_{Er} = 4.8$ K [10]). However, it has been recently observed that the hexagonal pseudo-ternary compound $TbFe_6Sn_4Ge_2$ was characterized by a small Tb–Fe coupling when Tb orders [11]. Therefore, it may be assumed that the R–T coupling results from a combination between the strength of the R–T interaction and the AF character of the T sublattice.

7. Conclusion

The replacement of manganese by iron in the hexagonal $ErMn_{6-x}Fe_xSn_6$ solid solutions pointed out two main features. The succession of the magnetic structures suggests an increasing antiferromagnetic character of the nearest interlayer interactions (J_1, J_2) yielding a reduction of the Er–T couplings and an increasing ferromagnetic next-nearest interaction (J_3). It should be now very interesting to study related solid solutions involving Ho and Tm to confirm the behaviour of the (Mn,Fe) sublattice and to check the play of R–T interactions of variable strength.

Another conclusion of this study is the change of the easy direction of the Er moment from easy plane to easy axis. It is known from magnetisation studies [5,6] that the in-plane anisotropy of erbium moment is weaker than the in-plane anisotropy of thulium. From this observation, it should be also interesting to study the behaviour of the thulium $TmMn_{6-x}Fe_xSn_6$ solid solutions. This may provide information on the origin of the magnetocrystalline anisotropy in the $HfFe_6Ge_6$-type compounds.

References

[1] G. Venturini, B. Chafik El Idrissi, B. Malaman, J. Magn. Magn. Mater. 94 (1991) 35.
[2] B. Malaman, G. Venturini, R. Welter, J.P. Sanchez, P. Vuillet, E. Ressouche, J. Magn. Magn. Mater. 202 (1999) 519.
[3] D.M. Clatterbuck, K.A. Gschneidner Jr, J. Magn. Magn. Mater. 207 (1999) 78.
[4] Y. Jin-lei, Z. Shao-ying, D. Juan, Y. Mi, Y. De-ren, Z. Li-gang, L. Shi-min, S. Bao-gen, Phys. Rev. B 67 (2003) 134423–134431.
[5] K. Suga, K. Kindo, L. Zhang, E. Brück, K.H.J. Buschow, F.R. de Boer, C. Lefèvre, G. Venturini, J. Alloys Compd. 408–412 (2006) 158–160.
[6] Y. Sawai, K. Kindo, L. Zhang, J.C.P. Klaasse, E. Brück, K.H.J. Buschow, F.R. de Boer, C. Lefèvre, G. Venturini, J. Alloys Compd. 408–412 (2006) 196–199.
[7] X.L. Rao, M.D. Coey, J. Appl. Phys. 81 (8) (1997) 5227, 2B.
[8] J.M. Cadogan, D.H. Ryan, J. Alloys Compd. 326 (2001) 166.
[9] J.M. Cadogan, D.H. Ryan, O. Moze, Suharyana, M. Hofmann, J. Phys.: Condens. Mater. 15 (10) (2003) 1757.
[10] J.M. Cadogan, Suharyana, D.H. Ryan, O. Moze, W. Kockelmann, IEEE Trans. Magn. 37 (4) (2001) 2006.
[11] K. Laura, D. Perry, H. Ryan, G. Venturini, B. Malaman, J. Alloys Compd. 436 (1–2) (2007) 1–8.
[12] B. Chafik El Idrissi, G. Venturini, B. Malaman, Mater. Res. Bull. 26 (12) (1991) 1331.
[13] O. Cakir, I. Dincer, E. Duman, T. Krenke, A. Elmali, Y. Elerman, J. Alloys Compd. 441 (2007) 19.
[14] J. Rodriguez-Carvajal, Physica B 192 (1993) 55.
[15] H. Shiraishi, T. Hori, N. Okkubo, K. Ohoyama, Phys. Stat. Sol. C 1 (12) (2004) 3660.
[16] C. Lefèvre, G. Venturini, B. Malaman, J. Alloys Compd. 346 (2002) 84–94.
[17] P. Schobinger-Papamantellos, G. André, J. Rodriguez-Carvajal, J.H.V.J. Brabers, K.H.J. Buschow, J. Alloys Compd. 226 (1995) 113.
[18] T. Mazet, O. Isnard, B. Malaman, J. Phys. Condens. Mater. 17 (2005) 1547.
[19] E.V. Rosenfeld, N.V. Mushnikov, Physica B 403 (2008) 1898.
[20] F. Canepa, R. Duraj, C. Lefèvre, B. Malaman, A. Mar, T. Mazet, M. Napoletano, A. Szytula, J. Tobola, G. Venturini, A. Vernière, J. Alloys Compd. 383 (2004) 10–16.